THE SURFACES OF LARISSA AND PROTEUS

PHILIP J. STOOKE
Department of Geography, University of Western Ontario, London, N6A 5C2, Canada

(Received 26 April 1994)

Abstract. Topographic models of Neptune's small inner satellites Larissa and Proteus were derived from the shapes of limbs and terminators in Voyager images, modified locally to accomodate large craters and ridges. The models are presented here in tabular and graphic form, including the first map of Larissa and the first detailed relief map of Proteus. The shape of Larissa is approximated by a triaxial ellipsoid with axes of 208, 192 and 178 km, but is only weakly constrained by the single available view. The volume is estimated to be $3.5 \pm 1.0 \times 10^6$ km^3. The surface is heavily cratered and may be crossed by one or two poorly seen linear ridges. Proteus is approximated by a triaxial ellipsoid with axes of 424, 390 and 396 km (the latter being the rotation axis dimension). The volume is estimated to be $3.4 \pm 0.4 \times 10^7$ km^3. Its surface appears to be very heavily cratered and extensive evidence for linear fractures is observed despite very low image quality.

1. Introduction

Larissa and Proteus, the largest of the small inner satellites of Neptune, were observed by the cameras of Voyager 2 in 1989 (Smith *et al.*, 1989) when they were referred to as 1989N2 and 1989N1 respectively. Thomas and Veverka (1990, 1991) described both satellites in more detail and presented a preliminary shape model of Proteus which they used to confirm synchronous rotation to within 5%. Croft (1992) examined the shape and geology of Proteus and published the first map of the satellite, showing craters and linear 'streaks' which he interpreted as valleys or troughs.

Despite low signal strength and limited coverage, I have used the Voyager images to create rough topographic models and maps of each satellite. Larissa has approximate dimensions of 208 by 192 by 178 km. The images reveal a number of large craters and possibly two linear ridges on one side of the satellite. Larissa appears to be as heavily cratered as Pandora, Janus or Epimetheus in the Saturnian system. Proteus is roughly 424 by 390 by 396 km in size and appears to be very heavily cratered. An extensive system of grooves or valleys is observed in the best image, and a large valley is tentatively identified in an earlier low resolution view. No features on Larissa have been given names by the International Astronomical Union, but the largest basin-like structure on Proteus has been provisionally named Pharos (Croft, 1992).

This report continues a series detailing the topography of non-spherical worlds. Previous studies, using the same techniques, include analyses of the jovian satellite Amalthea (Stooke, 1992a) and Saturn's co-orbital and F-Ring shepherd satellites (Stooke, 1993a, 1993b; Stooke and Lumsdon, 1993). The methods used are described fully in those reports and are only briefly reviewed in this paper.

Earth, Moon and Planets **65:** 31–54, 1994.

TABLE I
Voyager images of Larissa and Proteus

	FDS number	Spacecraft lat.	Spacecraft long.	Sub-solar lat.	Sub-solar long.	Phase angle	Scale (km/pixel)
Larissa							
	11381.42	−24	92	−24	117	22	4.1
	11381.48	−24	94	−24	119	22	4.1
Proteus							
A	11320.57	−27	275	−24	290	13	32.5
B	11321.03	−27	277	−24	292	13	32.5
C	11332.04	−27	35	−24	52	15	26.0
D	11332.10	−27	37	−24	54	15	26.0
E	11336.24	−27	65	−24	84	17	25.3
F	11336.30	−27	67	−25	86	17	25.3
G	11373.17	−27	94	−24	117	21	7.9
I	11373.28	−27	96	−24	119	21	7.9
H	11373.39	−27	99	−24	122	21	7.9
J	11373.50	−27	101	−24	125	21	7.9
	11389.20	4	334	−24	289	52	1.3

Note: letters at left identify images in Figure 2a. H and I are out of sequence because of the pairing of smeared and non-smeared images in Figure 2a.

2. Data

The Voyager 2 images of Larissa and Proteus used for this study are listed in Table I. A few additional disk-resolved images exist but are too small, noisy or smeared to be useful for shape modelling or mapping. Images are identified by FDS (Flight Data Subsystem) number. They were obtained on Planetary Data System (PDS) CD-ROMs from NASA's National Space Science Data Center.

Latitudes and longitudes given in this paper are planetocentric. The quoted latitudes assume a rotation axis perpendicular to the orbit plane, and the quoted longitudes assume synchronous prograde rotation. The prime meridian of each satellite faces Neptune and longitudes increase opposite to the direction of rotation, following planetary cartographic conventions. The Voyager images of Larissa comprise a single view and so cannot confirm these assumptions. The axis orientation and synchronous rotation of Proteus are confirmed in Voyager images spanning nearly two rotations, as explained below. The available information is insufficient to characterize any possible librations.

Voyager 2 obtained two images (FDS 11381.42 and 11381.48) which show surface features on the disk of Larissa. They are difficult to interpret on account of

low brightness levels and substantial noise, but they clearly show distinct craters. An earlier image, FDS 11354.43, is badly smeared. The two useful images were taken only a few minutes apart and show essentially the same view, so surface coverage is limited to about 40 percent of the satellite and stereoscopic viewing is not possible. In order to improve the signal to noise ratio, the two images were contrast stretched, enlarged and merged (Figure 1).

Proteus was observed in one high resolution frame (11389.20) with a resolution of 1.3 km/pixel, and a multispectral sequence of four images (11373.17 to 11373.50) with a resolution of 7.9 km/pixel. Several pairs of additional images were taken during approach with resolutions varying from 32 to 25 km/pixel, giving about 12 pixels across the disk in the poorest views used here (FDS 11320.57 and 11321.03). All Proteus images are low in contrast and noisy as a result of the short exposures (relative to the level of illumination) necessary to minimize smearing of the images. The northern limb in the highest resolution image was cut off by a data transmission error, but no more than a few lines were lost.

3. Method

The shapes of Larissa and Proteus were modelled from limb and terminator positions in the images listed in Table I, as described by Stooke and Keller (1990). Limb and terminator shapes were digitized from processed and enlarged images. Initial triaxial ellipsoid models of each satellite were created using the axis dimensions (208 by 192 by 178 km for Larissa, 440 by 416 by 404 km for Proteus) given by Thomas and Veverka (1991). The models were viewed and illuminated in the orientations given in Table I, registered to the shapes derived from the images, and modified to duplicate those outlines. Figure 3 shows the positions of limb and terminator traces on the map grids. Areas where several traces converge (e.g. around the south polar region of Proteus) are modelled most reliably, whereas regions not crossed by a limb or terminator are least reliable. An attempt was also made to model the shapes of ridges and craters which are seen on images but do not appear on a limb or terminator. Shapes of these features are essentially unconstrained, so contours in these regions are merely suggestive of the local topography.

Limbs are probably located to within about one pixel in the plane of each image, and terminators to within two or three pixels. With pixel dimensions of 20 or 30 km in some images there is room for very substantial uncertainty, caused primarily by smearing, aliasing effects at the limb, and the very low signal levels near terminators. When limbs are transferred to a body-fixed coordinate system for mapping, their locations may be uncertain by up to several tens of degrees perpendicular to the limb traces of Figure 3, reducing reliability in the model to no better than about twice the single pixel resolution of the original image even in the best areas.

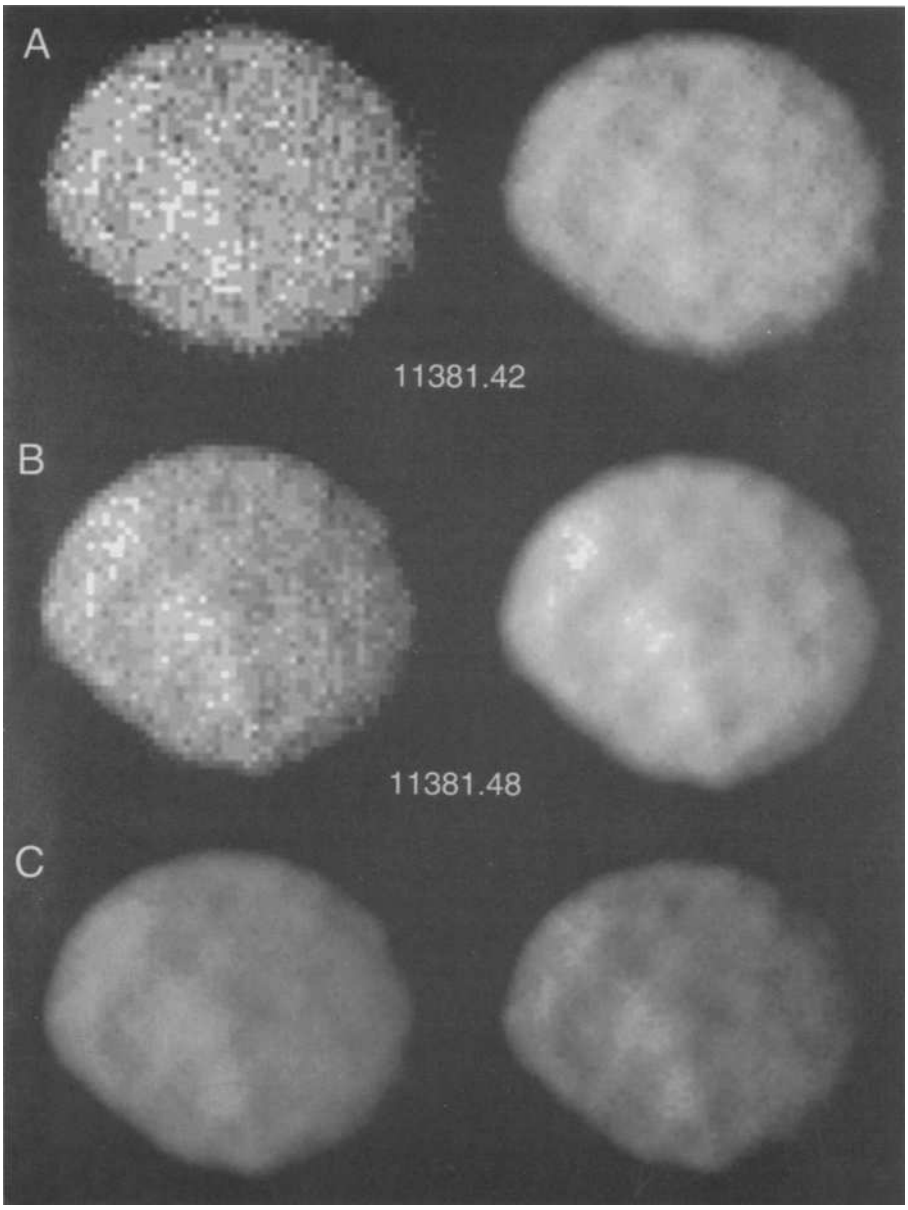

Fig. 1. A and B: Voyager images of Larissa, identified by FDS number. Left: original data. Right: original data merged with a smoothed version of itself. C: two versions of a composite of the original images. North is at top in this and all following images

Relative elevations near terminators may be more accurate since small variations in topography produce large changes in the shape of the terminator. Absolute radii near terminators are reasonably reliable only near limb traces, within

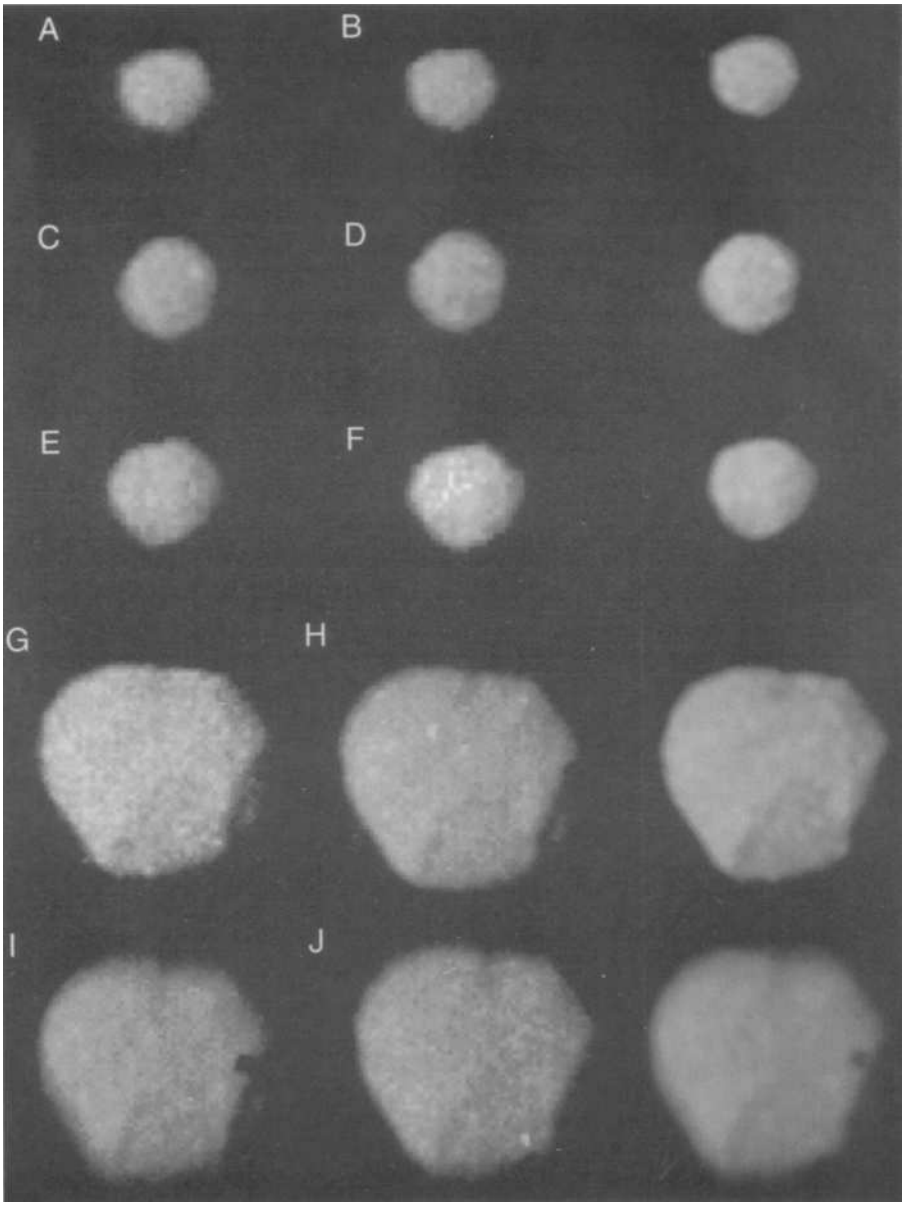

Fig. 2a.

the limits outlined above. Despite these considerable uncertainties, the models derived by these techniques are the best yet available since the low resolution and minimal overlap between images preclude stereoscopic imaging and control point triangulation. The radius matrices for the two models at the 5° spacing used

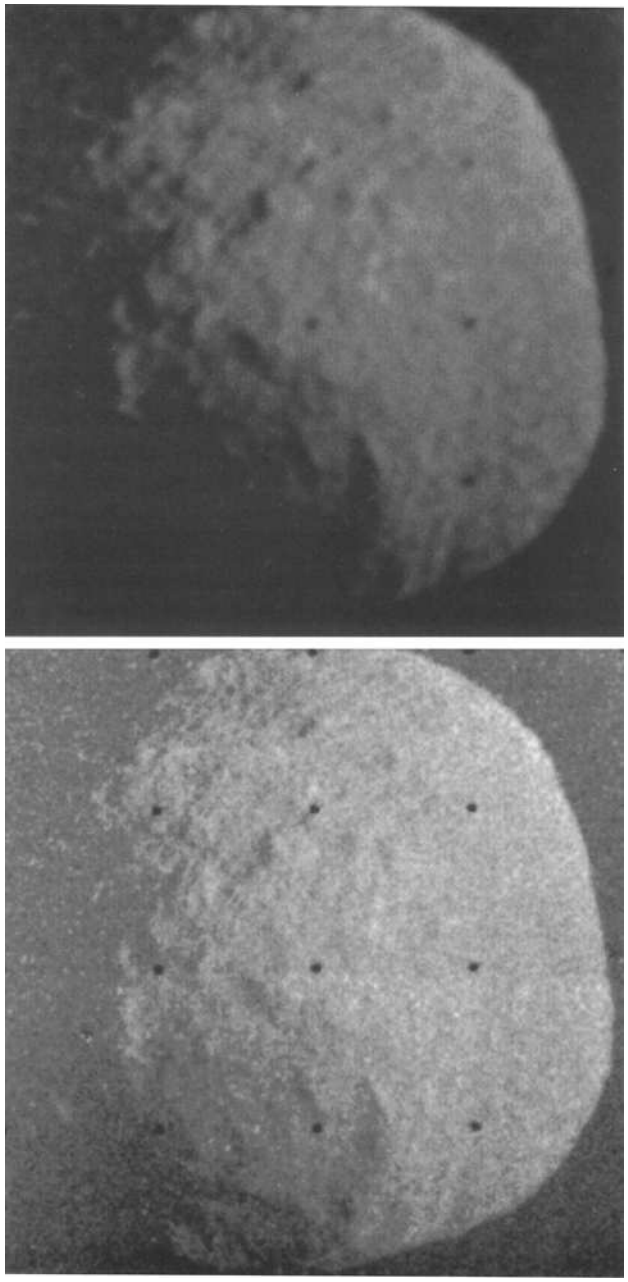

Fig. 2b.

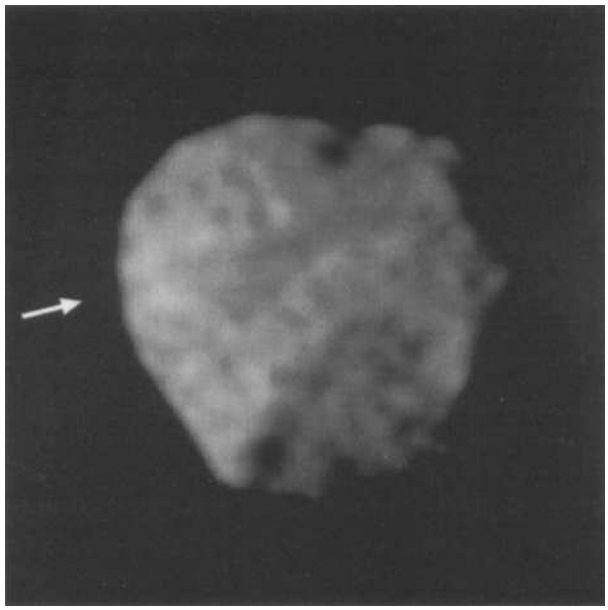

Fig. 2. (a) Low resolution images of Proteus. Letters identify images in Table I. Each row contains a pair of original images and, at right, a composite of the pair. The images in the bottom row are slightly smeared. (b) High resolution Proteus image FDS 11389.20. Two versions, each a composite of the original image with a smoothed version of itself to reduce the effects of noise. (c) Composite of images 11373.17 and 11373.39, processed to emphasize the possible linear valley (arrow).

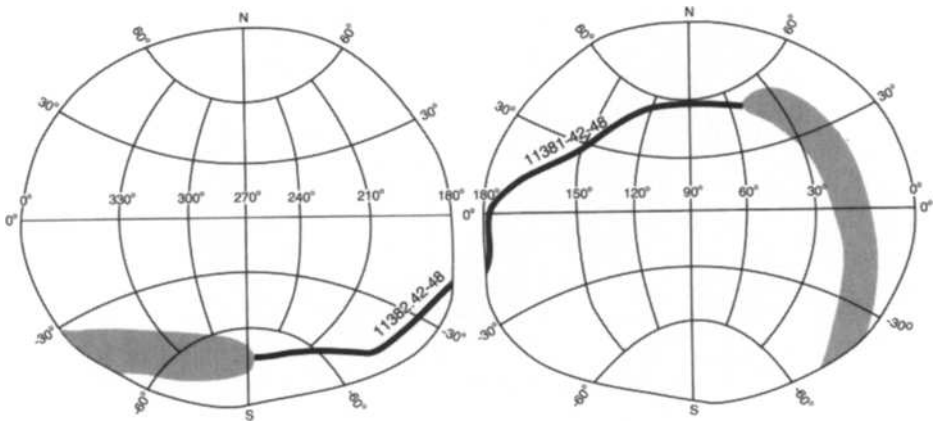

Fig. 3a.

during modelling may be obtained from the author on diskette or by electronic mail.

The maps presented here should be regarded as 'maximum interpretations'. They include features which I think necessary to account for subtle shadings in

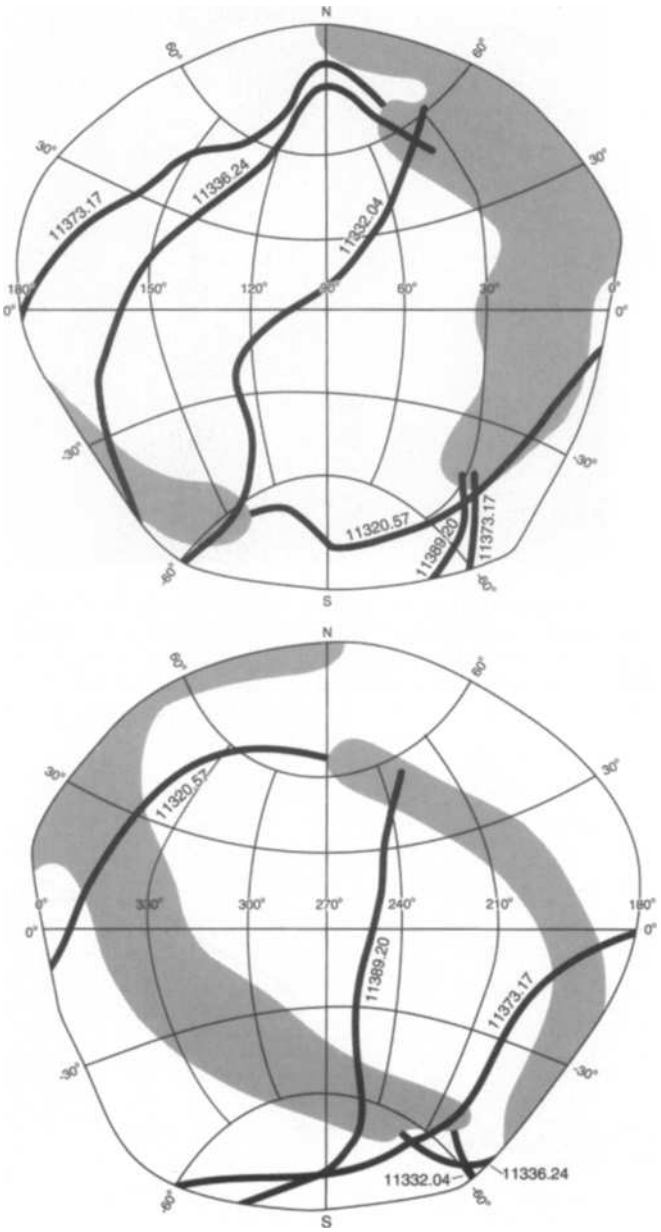

Fig. 3. (a) Locations on Larissa of the limb (solid line) and terminator (shaded area) used to derive the shape model. The map projection is the same as that used in Figure 6. (b) Locations on Proteus of the limbs (solid lines) and terminators (shaded areas) used to derive the shape model. The map projection is the same as that used in Figures 7, 8 and 10.

the noisy low contrast images. Other interpretations may differ in detail, but I believe there are reasonable grounds for including all features shown in these maps.

4. The Shape of Larissa

Since only one view of Larissa is available, the model is not unique and serves only as a rough guide to help prepare a map (Figure 6). For that reason, the model is not presented here in table or contour map form.

Larissa is slightly elongated, as clearly seen in Figures 1, 4 and 6. The north polar region, which is not visible in the images, is shown in Figure 6 as smooth and symmetrical. Hills near the pole would be visible in Voyager images, though large craters would be undetectable.

The maximum radius in the model is 10^6 km at 5° S, 10° W. The minimum radius is 81 km at 65° S, 225° W, in the depression which forms a prominent flat area on the southern limb. The equatorial diameter of the model from 0° to 180° longitude is 201 km, and the polar diameter of the model is 176 km. The volume of the model is $3.5 \pm 1.0 \times 10^6$ km^3. If a triaxial ellipsoid model of the shape is required, the axes suggested by Thomas and Veverka (1991), namely 208, 192 and 178 km, cannot be improved upon with the limited data in hand.

5. The Shape and Rotation of Proteus

The topographic model of Proteus is presented in Table II and illustrated in Figures 4, 5 and 7–10. Grids corresponding to five Voyager views are given in Figure 4 and six mutually perpendicular views are presented in Figure 5. Figure 7 is a shaded relief map of the surface of Proteus on a Morphographic Conformal projection (Stooke and Keller, 1990). The three dimensional convex hull of the model is the basis for the projection (Stooke, 1992b). In Figure 8 the shaded relief drawing has radius contours (measured in kilometres from the assumed centre of mass) superimposed. The area around the large crater Pharos is reprojected to the Simple Cylindrical map projection in Figure 9 to show the entire crater in one view.

The shape of Proteus was described by Smith *et al.* (1989) as slightly elongated, with topography of about 20 km on the limb. Thomas and Veverka (1991) described it as roughly ellipsoidal with semiaxes of 220, 208 and 202 km, and having regional variations of up to 15% (30 km) of the mean radius. Croft (1992) described the limb as roughly hexagonal in FDS 11373.17, squarish in 11389.20, and overall roughly ellipsoidal with semiaxes of about 215, 212 and 205 km. He indicated that it could be "almost as accurately described as simply a rugged spheroid 209 ± 8 km in radius" a view which is supported by the more detailed shape model described here. Proteus is not adequately described by any triaxial ellipsoid. It has several flat or slightly concave facets between 150 and 250

TABLE II

Radii of the Proteus model (km)

	Longitude									
	90	80	70	60	50	40	30	20	10	0
Latitude										
90	205.0	205.0	205.0	205.0	205.0	205.0	205.0	205.0	205.0	205.0
80	189.0	189.6	190.9	192.7	195.1	197.9	201.2	204.1	203.3	200.8
70	177.5	179.3	182.8	186.6	190.9	196.1	202.2	205.6	205.3	202.6
60	166.3	170.8	177.9	184.5	190.3	198.1	206.5	208.7	208.4	206.7
50	160.2	168.6	180.4	191.3	198.5	206.1	209.3	210.2	206.9	209.2
40	163.0	173.0	186.5	199.3	208.3	210.5	211.9	208.0	205.5	206.0
30	171.2	187.4	201.4	206.3	205.6	209.5	213.4	213.4	217.0	207.0
20	192.4	203.6	203.2	202.0	195.9	195.0	198.3	204.2	214.0	217.7
10	206.6	205.2	204.7	203.5	195.5	191.9	193.8	199.4	204.0	210.0
0	199.7	198.8	205.1	207.7	202.9	198.0	196.0	195.9	192.5	194.7
−10	199.9	203.6	206.4	211.0	205.0	204.9	198.9	192.0	193.0	194.7
−20	204.9	204.9	209.1	211.2	214.3	208.0	198.0	198.6	195.0	196.9
−30	205.3	207.9	205.0	193.5	201.1	214.5	206.0	210.0	205.5	197.9
−40	201.3	200.6	199.4	187.4	203.3	224.5	214.0	208.1	203.7	202.3
−50	184.1	181.9	188.8	197.2	205.8	213.8	218.0	223.4	223.4	215.7
−60	179.1	179.7	186.6	195.5	201.1	205.7	209.3	208.0	211.2	209.3
−70	187.6	188.0	189.7	192.7	196.8	201.3	203.3	204.0	204.2	204.1
−80	195.2	196.2	197.3	198.0	198.6	199.2	199.8	199.8	199.7	200.1
−90	200.3	200.3	200.3	200.3	200.3	200.3	200.3	200.3	200.3	200.3
	Longitude									
	180	170	160	150	140	130	120	110	100	90
Longitude										
90	205.0	205.0	205.0	205.0	205.0	205.0	205.0	205.0	205.0	205.0
80	204.6	202.4	200.1	197.9	195.4	193.1	191.2	189.9	189.1	189.0
70	203.4	202.2	198.3	194.7	191.3	188.4	185.0	181.0	178.0	177.5
60	203.6	205.5	202.6	201.5	197.5	193.1	185.1	176.5	169.3	166.3
50	208.0	208.5	212.6	211.9	205.4	196.1	185.1	172.6	161.6	160.2
40	212.2	215.2	215.9	211.6	203.2	199.0	187.8	175.0	163.1	163.0
30	219.8	224.1	222.9	213.6	207.6	202.0	191.5	183.4	171.1	171.2
20	224.3	229.9	229.8	219.5	211.9	204.9	198.7	198.9	192.4	192.4
10	223.9	229.6	229.1	220.6	208.1	197.2	196.1	203.9	204.9	206.6
0	218.7	224.7	224.6	215.9	201.7	195.7	197.7	203.5	203.0	199.7
−10	209.2	210.0	210.5	205.1	194.5	194.3	195.4	195.0	200.8	199.9
−20	197.9	207.5	200.7	194.3	191.3	194.7	198.5	202.5	204.4	204.9
−30	191.1	198.8	198.4	191.7	190.8	194.8	200.3	203.0	204.2	205.3
−40	192.5	196.0	194.6	189.1	190.0	195.7	200.8	204.2	205.0	201.3
−50	199.0	200.1	197.9	195.3	195.5	199.5	203.7	204.8	192.4	184.1
−60	205.2	204.2	203.0	201.7	200.8	203.0	203.6	196.2	184.6	179.1
−70	200.6	200.8	201.2	201.1	199.9	198.7	195.4	193.2	189.4	187.6
−80	187.3	187.4	188.4	190.2	192.3	192.9	193.4	193.4	193.7	195.2
−90	200.3	200.3	200.3	200.3	200.3	200.3	200.3	200.3	200.3	200.3

TABLE II

Continued

	Longitude									
	270	260	250	240	230	220	210	200	190	180
Latitude										
90	205.0	205.0	205.0	205.0	205.0	205.0	205.0	205.0	205.0	205.0
80	196.9	199.3	200.9	201.8	203.0	203.6	204.0	204.4	204.9	204.6
70	184.7	188.5	193.6	197.8	198.6	200.7	201.3	201.3	201.9	203.4
60	182.6	187.8	192.6	194.8	197.1	200.2	200.6	201.4	202.6	203.6
50	188.3	195.5	197.9	200.2	202.7	202.1	202.9	205.0	206.8	208.0
40	197.4	202.5	203.5	203.8	202.9	202.4	203.5	206.6	210.1	212.2
30	201.8	203.7	203.8	204.3	203.7	203.4	204.4	208.2	212.4	219.8
20	192.5	198.9	201.5	203.6	205.6	205.4	206.2	210.0	215.2	224.3
10	188.5	189.0	192.5	196.3	200.8	205.8	209.3	211.8	216.4	223.4
0	192.0	191.0	190.0	191.1	196.2	205.1	213.0	214.9	214.1	218.7
−10	193.3	191.0	188.5	189.1	194.9	204.5	208.6	204.6	202.6	209.2
−20	196.4	194.2	190.6	191.1	196.5	201.1	195.5	190.1	190.3	197.9
−30	201.2	198.9	196.2	196.6	200.5	198.4	189.6	183.0	183.8	191.1
−40	210.1	206.1	202.5	202.6	206.4	200.4	190.9	185.7	186.3	192.5
−50	206.6	207.6	208.8	209.5	208.2	206.0	200.1	196.4	196.8	199.0
−60	203.4	206.5	209.6	211.6	211.7	210.1	209.3	208.6	207.1	205.2
−70	203.6	205.2	206.9	208.9	210.4	209.7	208.0	206.0	202.7	200.6
−80	207.5	207.6	207.7	204.7	201.4	196.3	192.4	189.8	188.1	187.3
−90	200.3	200.3	200.3	200.3	200.3	200.3	200.3	200.3	200.3	200.3
	Longitude									
	360	350	340	330	320	310	300	290	280	270
Latitutde										
90	205.0	205.0	205.0	205.0	205.0	205.0	205.0	205.0	205.0	205.0
80	200.8	198.4	196.3	194.4	193.7	193.3	193.0	194.4	195.5	196.9
70	202.6	197.6	193.2	189.2	186.7	184.9	184.0	182.6	182.5	184.7
60	206.7	202.0	194.0	186.3	181.0	174.5	172.5	173.8	177.2	182.6
50	209.2	204.3	197.7	192.3	187.6	180.2	175.4	176.0	180.7	188.3
40	206.0	199.8	195.7	194.3	193.8	190.1	187.3	186.1	189.8	197.4
30	207.0	208.0	200.5	204.0	201.8	200.1	199.5	200.1	201.8	201.8
20	217.7	217.6	215.5	211.5	207.8	205.7	196.5	192.3	195.0	192.5
10	210.0	221.2	222.7	218.0	216.3	210.4	198.6	193.3	193.4	188.5
0	194.7	201.5	219.1	218.3	210.0	213.2	205.3	200.1	196.7	192.0
−10	194.7	193.1	203.2	215.0	213.5	211.4	204.5	200.3	196.8	193.3
−20	196.9	191.6	197.3	212.0	210.1	207.7	204.8	202.5	199.8	196.4
−30	197.9	191.5	195.2	206.7	202.1	198.5	198.0	203.3	204.8	201.2
−40	202.3	196.1	204.4	202.5	195.8	193.7	194.8	202.4	207.8	210.1
−50	215.7	208.4	205.8	202.0	194.5	190.2	193.2	199.5	205.9	206.6
−60	209.3	204.4	198.4	195.0	191.8	192.2	193.6	197.8	200.5	203.4
−70	204.1	203.4	198.8	193.7	192.0	193.0	196.4	200.7	202.2	203.6
−80	200.1	200.7	203.0	204.1	204.4	205.5	206.5	207.4	207.4	207.5
−90	200.3	200.3	200.3	200.3	200.3	200.3	200.3	200.3	200.3	200.3

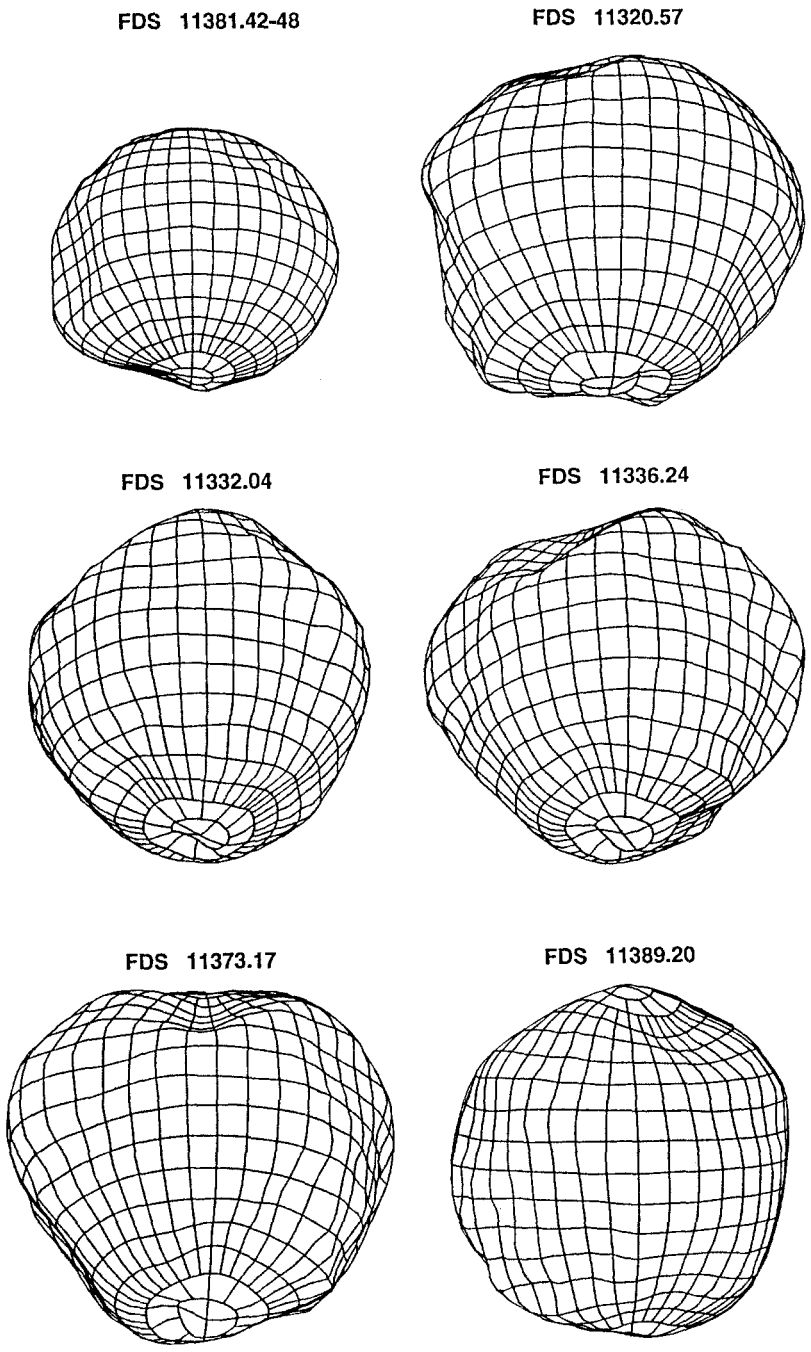

Fig. 4. Latitude-longitude grids in orthographic projection corresponding to the single Voyager view of Larissa (top left) and five images of Proteus (remaining grids), not to the same scale. See Table I for further details.

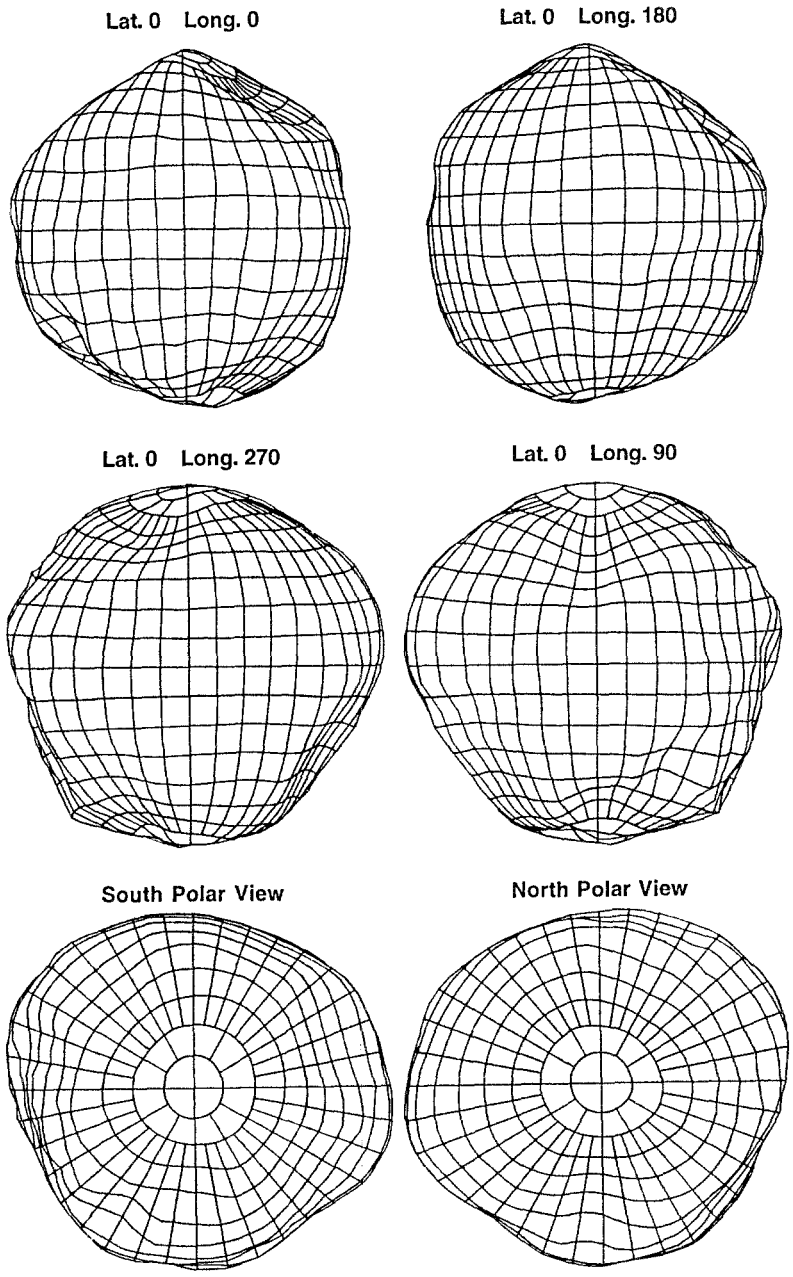

Fig. 5. Orthographic latitude-longitude grids representing Proteus, viewed from six mutually perpendicular directions.

km in diameter, presumably created by very large impacts. The facets appear as large craters in the shaded relief drawing (Figures 7 and 8), as depressions in the

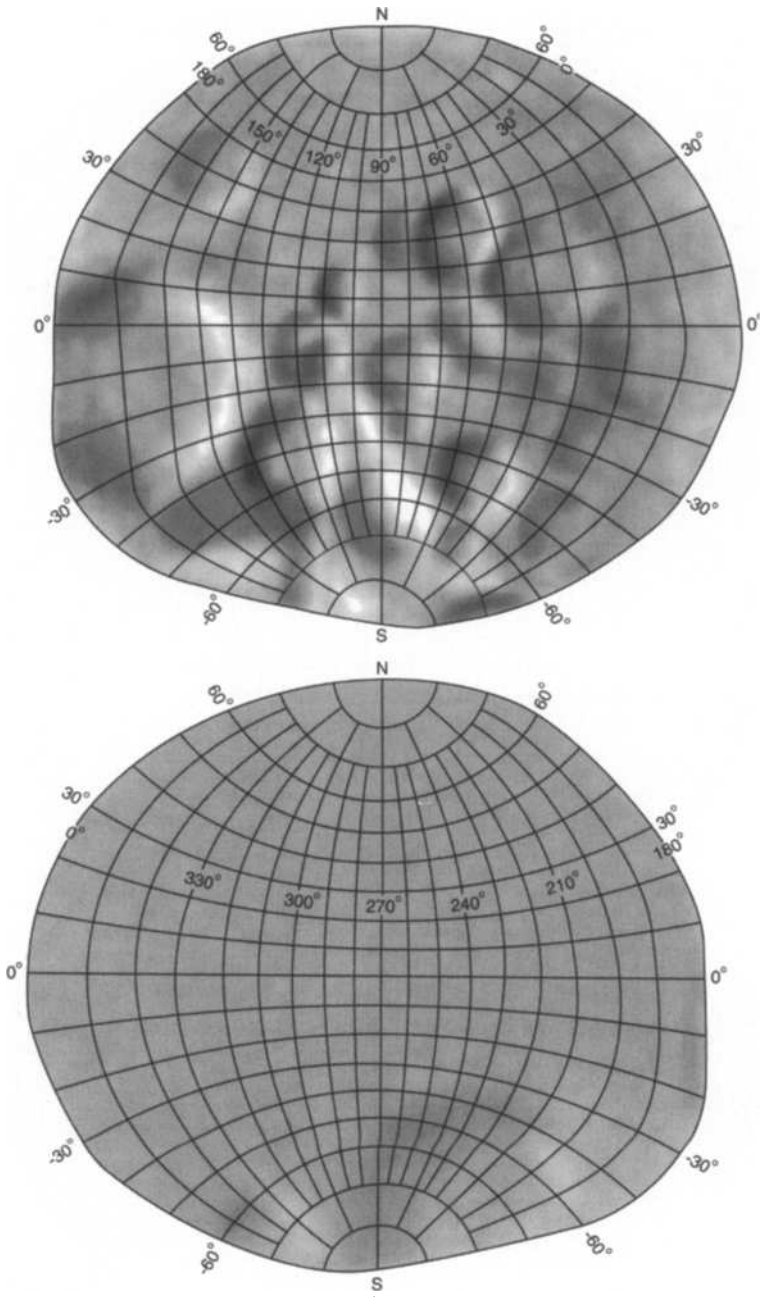

Fig. 6. Shaded relief map of Larissa on the Morphographic Conformal Projection.

contour map (Figure 8) and as dashed circles in Figure 10. They are responsible for the polygonal outlines seen in Figures 2a and 2b.

The lower resolution Proteus images were merged where appropriate to reduce the effects of noise. Visual comparison of the raw images shows that limbs vary in shape from pair to pair, but that limbs in any one pair are effectively identical (Figure 2a). This indicates that all the images listed in Table I contain useful information about the global shape of Proteus. Thomas and Veverka (1990; 1991) made use of only the last three imaging sequences, and Croft (1992) used only the last two, but I have used the last five for this study. The previous reports state that no surface features can be reliably identified in the low resolution image pairs, but when the images are combined to reduce noise some features may be revealed.

The four-image multispectral sequence includes two sharp images (11373.17 and 11373.39) and two which are slightly smeared (Figure 2a). The two sharp images were contrast stretched and merged to reduce noise, revealing an unexpected linear feature (arrow in Figure 2c). It is difficult to be certain of its reality, but I consider it likely to exist and show its position on the map of Proteus (Figure 7).

The highest resolution image of Proteus has extremely low contrast and considerable noise. The versions printed here (Figure 2b) are composites of the original image and a smoothed copy of itself. The smoothing reduces the effects of noise, while the original data preserve the full resolution of the image without entirely undoing the effects of the smoothing, and the result is sometimes easier to interpret than the original data.

The maximum radius in the model is 232.5 km at 15° N, 165° W. The minimum radius is 159.5 km at 50° N, 95° W. This occurs at the centre of a large flattened 'facet', presumably an ancient degraded crater some 200 km across. It is seen in profile at upper left in Figure 2a (C and D) and its depth may be uncertain by as much as 20 km. The equatorial diameter of the model from 0° to 180° longitude is 413.4 km. The maximum dimension parallel to this line is 423 km at 15° N. From 90° to 270° the equatorial diameter is 391.7 km, and the polar diameter of the model is 405.3 km. Figure 2a clearly shows the variation in equatorial dimensions, since the ratio of polar to equatorial widths at low phase angle in images C and D is noticably less than in A, B, E and F. The volume of the model is $3.4 \pm 0.4 \times 10^7$ km^3. If a triaxial ellipsoid model is required, semiaxes of 212, 195 and 198 km give a reasonable approximation to the shape and volume. Those dimensions are given in the common 'a, b, c axis' order, where c is the rotation axis. The fact that the rotation axis is not the smallest of these dimensions is a reflection of the error introduced by trying to fit a triaxial ellipsoid model to the lumpy shape of Proteus.

Synchronous rotation is confirmed by the images. Thomas and Veverka (1990) had noted that the position of Pharos in images 11373.17 and 11389.20 was consistent with synchronous rotation to within 5% of the orbital period. The lower resolution images appear to strengthen the case. Figure 2a (E, F and the composite of the two) shows a faint dark region near the terminator which matches the

size of Pharos and the position expected for synchronous rotation. Smaller dark patches occur in the same images at the expected locations of the crater at 15° N, 40° W and the large depression centred at 60° S, 60° W. Both are clearly visible in Figures 2a (G and H) and 2c. Figure 2a (C, D and the composite of them) show a dark shading in the southern part of the terminator at the expected position of a broad valley southeast of Pharos and parallel to its rim, which is clearly seen near the south limb in Figure 2b.

If these low resolution images and the processing used to create Figure 2 are being interpreted correctly, the rotation was prograde (which was not demonstrated by previous studies) and must have been within about ±30° of the 600° expected for synchronous rotation during the period spanned by these images. Prograde rotation is further suggested by the appearance of a small part of the domed floor of Pharos beyond the terminator in image 11373.17. By the time image 11373.39 was obtained, after 5° of rotation, the illuminated patch had become distinctly smaller as expected for prograde rotation.

6. Surface Features of Larissa

The shaded relief drawing shows several prominent craters. The largest, near the anti-Neptune point, is about 90 km across. There are several well defined craters with diameters in the 30 to 40 km range, and other possible craters of this size suggested by shading or depressions in the limb and terminator. The less certain craters are drawn less distinctly on the maps. Noise gives the impression of a rugged surface with craters near the limit of resolution. The reality of small features in the Larissa images is very difficult to determine. I have tried to avoid indicating a crater on Figure 5 unless it is reasonably well seen in both original images. Other interpretations of these images may differ in detail from that presented here. For this reason, as well as the low resolution, no attempt is made here to investigate crater densities and estimate surface ages.

Apart from craters, the only topographic features revealed in the Voyager images are a pair of faint linear structures whose very existence is far from certain. One extends about 100 km from 20° S, 100° W to 60° S, 30° W and is apparently a ridge. Bright patches occurring along it (but nowhere else on Larissa) may be caused by albedo markings as well as by sun-facing slopes, though the resolution is too poor to be certain. The other linear feature runs from 10° N, 95° W to 60° S, 110° W, and possibly extends to the south limb at 75° S, 180° W. This resembles a broad valley of varying width (stated positions are for the eastern edge), but it may be no more than a chance alignment of craters.

7. Surface Features of Proteus

The surface of Proteus is heavily cratered. Apart from the facets described above, there are several craters with diameters in the 60 to 100 km range and more in the best image with diameters of 20 to 50 km. The highest resolution (1.3 km/pixel) image suggests the presence of many craters with diameters of 8 to 15 km, but the extremely low contrast and excessive noise render identification of individual craters uncertain. Since other interpretations of craters and their diameters may differ in detail from mine, no crater size distribution statistics are attempted here.

The largest crater or basin, Pharos (Figure 9), is really one of the facets already described, but it warrants special attention because it dominates the best image. Its diameter is approximately 230 km. The floor is not concave but is gently domed in the centre with an annular trough below the walls. This doming is apparent because the shadow in the interior, in image 11389.20, lies on the west side, not the east as would be expected for a concave crater. The central dome appears intermediate in form between the floor of the lunar crater Ptolemaeus (which has roughly the same curvature as the lunar mean) and the prominent central massif of Odysseus on Tethys. A scarp facing west (towards the interior of Pharos) at 348° W between latitudes 10° S and 30° S is probably part of the outer wall displaced inwards as a giant terrace, since the main rim to the east is lower here than elsewhere. The depth of Pharos is only weakly constrained. The wall heights in the shape model (from 10 to 15 km) are very rough estimates. Croft (1992) estimated wall heights of 10 km.

Images 11373.17 to 11373.50 (Figure 2a, G to J) show Pharos on the terminator. Just to the east, part of the domed crater floor rises into sunlight. Croft (1992) interpreted this incorrectly as the eastern rim of Pharos, though it may include part of the eastern wall of the largest crater to overlap Pharos, a 100 km diameter crater at 40° S, 20° W. In image 11389.20 a faintly illuminated region was noted by Croft (1992) and interpreted as part of the western rim of Pharos. Detailed modelling of this region suggests that the illuminated spot is at 5° S, 40° W, on a high point just outside the rim between several other craters.

At 5° S, 0° W on the northern floor of Pharos a faint circular patch, apparently a hill or dome, may be discerned in image 11389.20. It has a diameter of about 20 km. The description of this as a dome does not imply a volcanic origin. Volcanism would not be expected on an object the size of Proteus, particularly since its non-spherical shape suggests it has never experienced significant heating.

Several depressions surround Pharos, particularly a north-south oriented valley on longitude 310° W just outside the south-east rim of Pharos (Figure 2b), a major facet or depression at 60° S, 60° W (Figure 2c) and a large subdued crater at 20° N, 40° W. Shading in image 11389.20 suggests that a ridge runs south-eastwards from 60° N, 0° W to 30° N, 300° W, parallel to the northeastern rim of Pharos. One possible interpretation of all these features is that they constitute an outer trough and ring of Pharos itself. The trough would be roughly 150 km

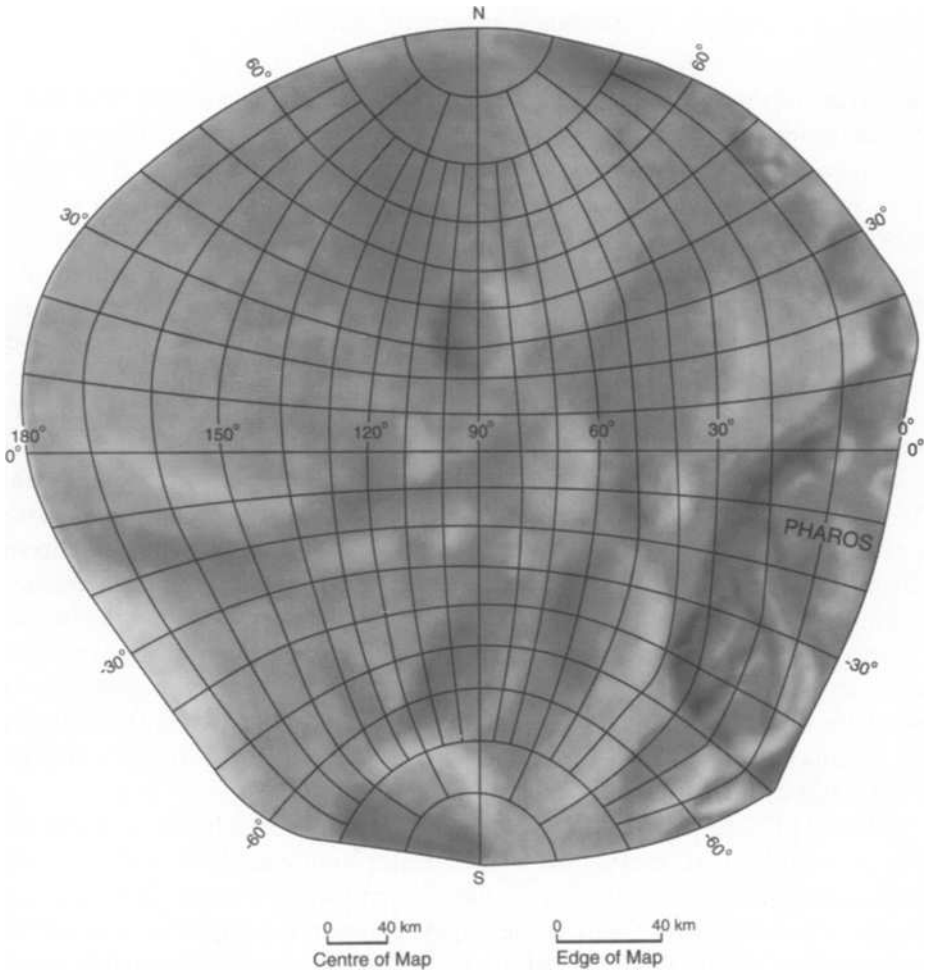

Fig. 7. Shaded relief map of Proteus on the Morphographic Conformal Projection.

wide, giving a total diameter of between 500 and 550 km for the Pharos structure. This, of course, is substantially greater than the present diameter of Proteus, though only about 40% of its mean circumference. The existing images and shape model are not adequate to confirm this suggestion, but the partial relaxation of Proteus after such a massive impact might account for the substantial degree of fracturing observed on Proteus and described below.

Numerous grooves or valleys are visible in the images and maps of Proteus. The most prominent on the map is the large valley mentioned above (Figure 2c, arrowed), extending from 10° S, 180° W to 10° S, 90° W. If this is not an artifact of the processing technique described above, it is a major structural feature. The same processed image weakly shows other linear features not included in the map, particularly one running diagonally across Figure 2c from lower left to

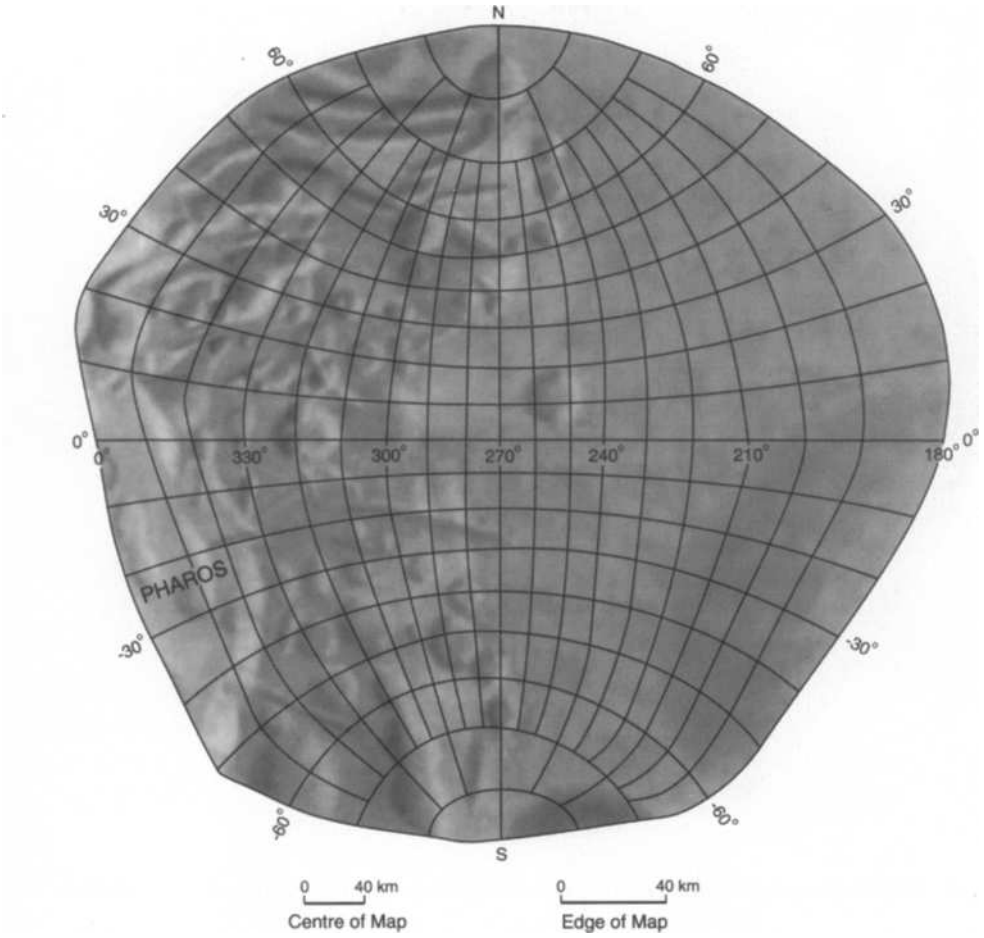

Fig. 7. Continued.

the centre of the disk (40° S, 180° W to 10° S, 90° W). I regard this as too uncertain to show in the map. The large valley is probably the result of a major facet-forming impact.

The remaining grooves and linear features shown in Figures 7–10 are mapped from image 11389.20. Many are found north and east of Proteus, near the north pole. Croft (1992) cautions that linear artifacts may occur under these lighting and viewing conditions. Caution is certainly required, but similar lineations are not seen on Prometheus or Janus under similar conditions (Stooke 1993a; Stooke and Lumsdon 1993). Several other lineaments are indicated in Figures 7 to 10. The less certain ones are shown as dashed lines in Figure 10. Some may be chance alignments of bright or dark pixels, similar to a printer's so-called 'rivers' in blocks of text which are caused by the juxtaposition of spaces between words in adjacent lines. These do occur occasionally in areas beyond the limb, but so

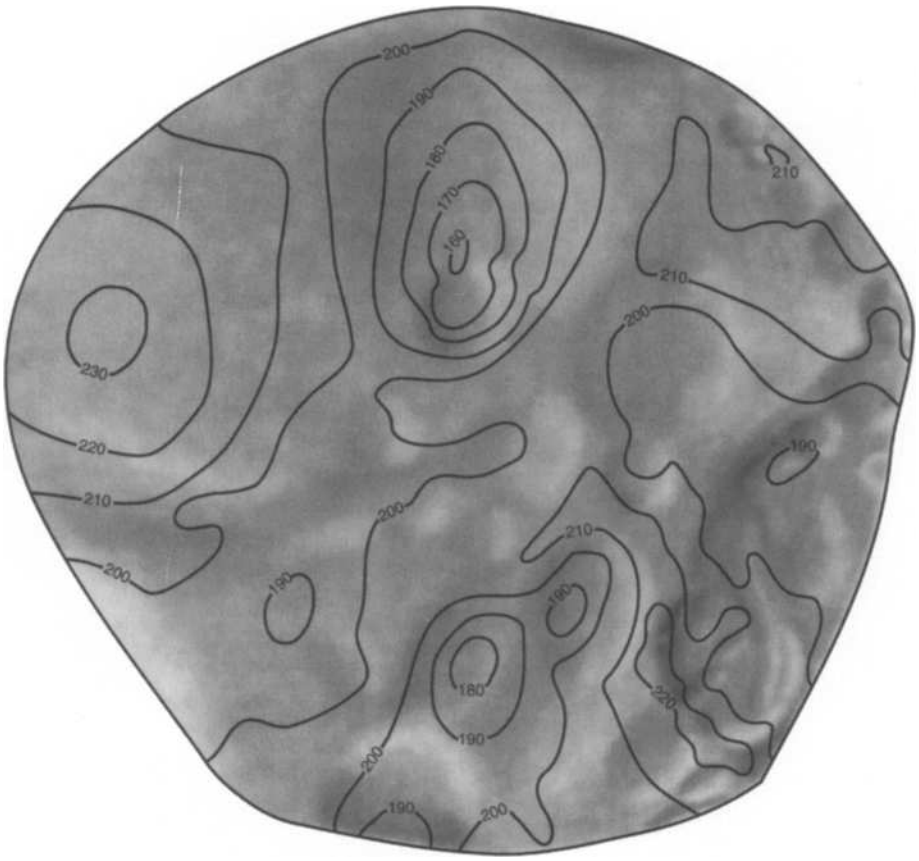

Fig. 8. Shaded relief map of Proteus with contours of local radius in kilometres at 10 km intervals.

rarely that they are not likely to be the cause of all the linear features observed on Proteus. Most lineaments are probably real features which are hard to discern through the noise, so confidence in their reality is low. Despite these problems, and while the reality of individual lineaments or the global pattern of distribution may be uncertain, it is clear that Proteus has many narrow grooves.

One particularly interesting groove or valley occurs within Pharos, where it runs about 100 km from 45° S, 10° W to 20° S, 30° W. It may extend further north along the terminator. This groove is roughly 12 km wide and appears flat-floored, like a well-defined graben. It crosses the northern rim of the 100 km diameter crater on the southwestern floor of Pharos, where its apparent winding course in Figure 2b may be in part due to the high relief of this area.

Croft (1992) mapped several broad streaks which he interpreted as troughs and attributed to the giant Pharos impact. Some of his streaks (A, B and C in his Figure 4) correspond to features mapped as craters in Figure 7. They are elongated north to south in some images by smearing, which contributes to a

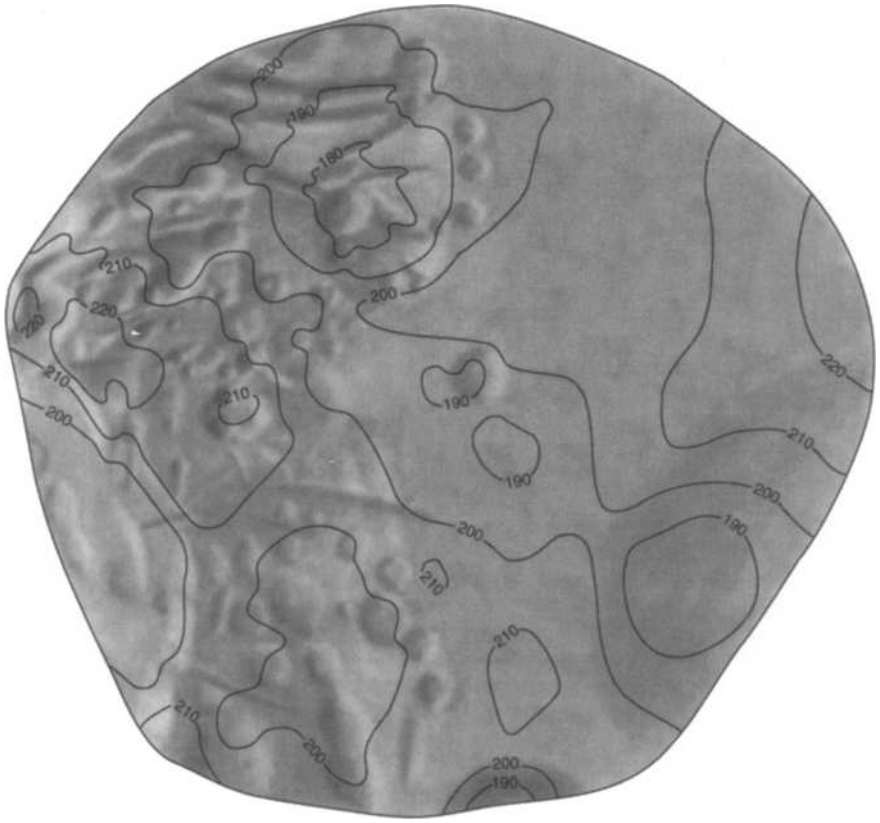

Fig. 8. Continued.

streak-like appearance. The large valley shown in Figure 2c was not identified by Croft, and others of his streaks are not identified here, an indication of the difficulty of interpreting these images. The broad valley southeast of Pharos, centred on the 310° meridian, is Croft's "streak F" (strictly speaking, his streak corresponds to the crater chain mapped here in the centre of the much wider valley). Croft suggested that several streaks formed a concentric ring around Pharos, similar to the possible outer ring of depressions mentioned above. These two possible outer structures are composed of different combinations of features, but some are common to both (especially "streak F"). The structural effects of relaxation of hemisphere-sized craters need to be investigated further to advance our understanding of Proteus.

Albedo markings are not obvious in the images. All changes in brightness may be explainable topographically, but several areas may exhibit modest albedo variations which contribute to brightness changes in the images. Given the poor quality of the images themselves, even photometry applied to the shape model may be unable to isolate real albedo variations. If any exist, the following are

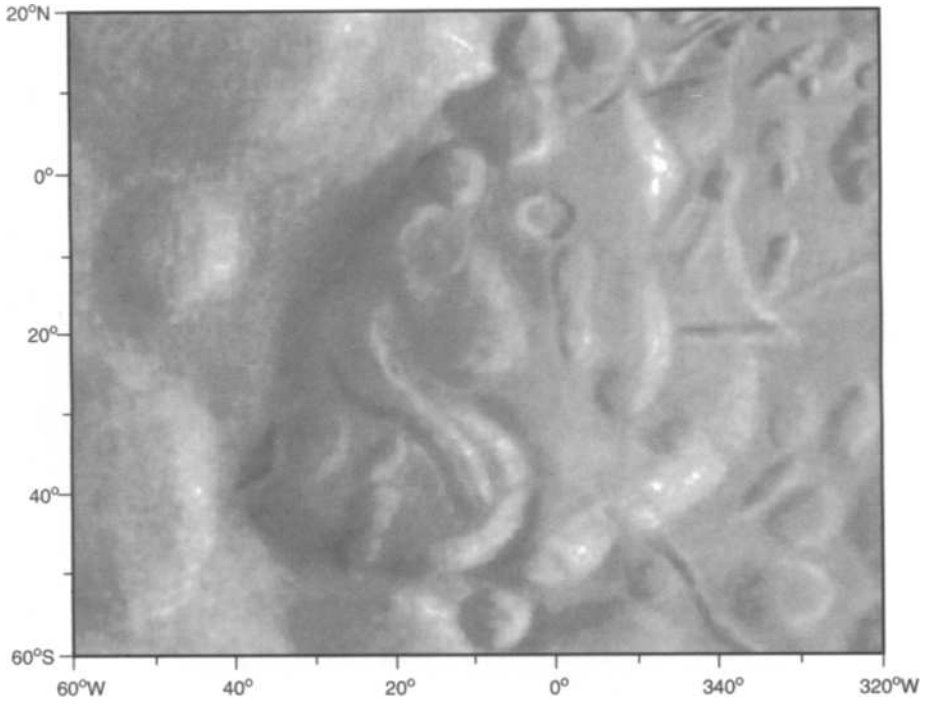

Fig. 9. The region around the crater Pharos, reprojected from Figure 7 to a simple cylindrical projection.

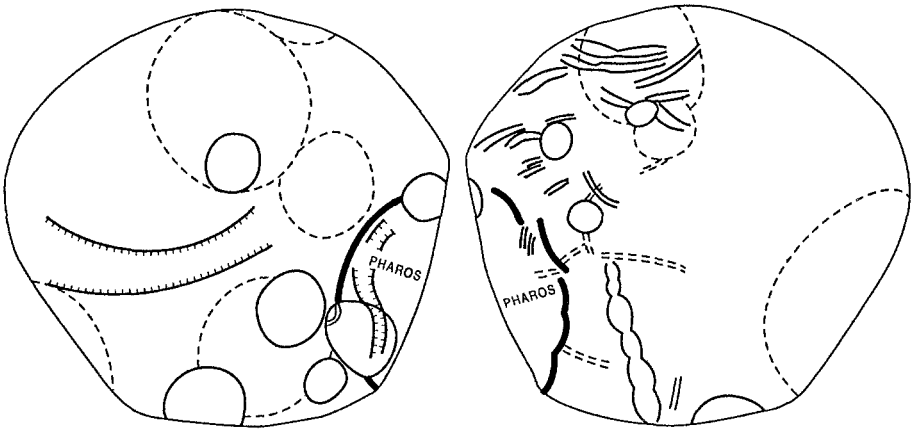

Fig. 10. Major surface features of Proteus. Dashed loops: large facets, degraded craters. Solid loops: prominent craters. Heavy solid arcs: rim segments of Pharos crater. Light double lines: grooves, valleys. Heavy double lines: large graben or valleys (ticks point downslope). Scalloped double line: crater chain. Dashed double lines: uncertain grooves.

likely candidates. First, the large depression at 60° S, 60° W appears darker than other areas of the disk seen at similar distances from the terminator in Figures 2a (images E to J) and 2c. This may be due to topography, but that would require the depression to have a high ridge along its western edge (longitude 100° W) and a steep overall tilt to the southeast across its floor. That is not impossible, but it suggests a quite different shape in this region and may be hard to reconcile with the (admittedly low resolution) limb in Figure 2a (C and D). Second, similar comments might be made about the interior of Pharos itself, seen in Figures 2b and 2a (E and F). In the latter images, and more so in the composite of the two, the floor of Pharos appears slightly darker than its surroundings. The reality of this tentative suggestion is very uncertain. Third, a similar interpretation might be given to the region around 40° N, 280° W as seen in Figure 2b. It is shown in the relief drawing as a subdued crater, but its floor appears slightly darker than its surroundings and this may not be entirely due to topography.

Fourth, a crater about 20 km in diameter at 30° N, 327° W may be a little brighter than its immediate surroundings. In some processed versions of this image it resembles a bright ring. This may be due to a chance location on the sun-facing side of a hill, but may also indicate bright (possibly fresh) ejecta. If so it is the only bright ejecta deposit identified on either Proteus or Larissa. Finally, Figure 2c shows bright patches at the left (west) limb on the sides of the possible valley, and a darker valley floor. This pattern is typical of valleys seen at low phase angles on Phobos (Thomas, 1979) and Epimetheus (Stooke, 1993b). Some of the difference in brightness may be caused by particle size or texture variations, but it may also reflect real albedo variations perhaps due to the exposure of fresh material by mass wasting on the valley walls. Without a better model of the valley's topography for photometric analysis, the reality of albedo variation cannot be established.

These observations are inconclusive but indicate that, while albedo variations cannot be confirmed, they may occur in several specific locations on Proteus. Definitive measurements of albedo must await future visits to the Neptunian system.

Conclusion

The available Voyager images of Proteus and Larissa are so limited in number and contrast that interpretation is difficult. However, they are likely to be the only images available for several decades. The preceding discussion is often qualified as uncertain, and several suggestions (an outer ring of Pharos, a large valley on the leading side, faint albedo variations) may be impossible to substantiate with current data. However, more might be done with new techniques of image enhancement, as was attempted here for the first time. The availability of pairs of images was particularly useful, and this imaging strategy should be considered whenever possible in similar situations in future.

Acknowledgements

The images used for this study were provided courtesy of the National Space Science Data Center, NASA's Planetary Data System and Dr. B.A. Smith, leader of the Voyager Imaging Team. I thank Diane Shillington for help with the manuscript and David Mercer for his valued cartographic support.

References

Croft, S. K.: 1992, *Icarus* **99**, 402–419.

Smith, B. A., Soderblom, L. A., Banfield, D., Barnet, C., Basilevsky, A. T., Beebe, R. F., Bollinger, K., Boyce, J. M., Brahic, A., Briggs, G. A., Brown, R. H., Chyba, C., Collins, S. A., Colvin, T., Cook, A. F., Crisp, D., Croft, S. K., Cruikshank, D., Cuzzi, J. N., Danielson, G. E., Davies, M. E., De Jong, E., Dones, L., Godfrey, D., Goguen, J., Grenier, I., Haemmerle, V. R., Hammel, H., Hansen, C. J., Helfenstein, C. P., Howell, C., Hunt, G.E., Ingersoll, A. P., Johnson, T. V., Kargel, J., Kirk, R., Kuehn, D. I., Limaye, S., Masursky, H., McEwan, A., Morrison, D., Owen, T., Owen, W., Pollack, J. B., Porco, C. C., Rages, K., Rogers, P., Rudy, D., Sagan, C., Schwartz, J., Shoemaker, E. M., Showalter, M., Sicardy, B., Simonelli, D., Spencer, J., Sromovsky, L. A., Stoker, C., Strom, R., Suomi, V. E., Synott, S. P., Terrile, R. J., Thomas, P., Thompson, W. R., Verbiscer, A. and Veverka, J.: 1989, *Science* **246**, 1422–1449.

Stooke, P. J.: 1992a, *Earth, Moon and Planets* **56**, 123–139.

Stooke, P. J.: 1992b, *Proceedings, International Conference on Asteroids, Comets, Meteorites 1991*, Flagstaff (Harris, A. W. and Bowell, E., eds.), 583–586. Houston: Lunar and Planetary Institute.

Stooke, P. J.: 1993a, *Earth, Moon and Planets* **62**, 199–221.

Stooke, P. J.: 1993b, *Earth, Moon and Planets* **63**, 67–83.

Stooke, P. J. and Lumsdon, M. P.: 1993, *Earth, Moon and Planets* **62**, 223–237.

Stooke, P. J. and Keller, C. P.: 1990, *Cartographica* **27**, 82–100.

Thomas, P.: 1979, *Icarus* **40**, 223–243.

Thomas, P. C. and Veverka, J.: 1990, *Reports of Planetary Geology and Geophysics Program – 1989*, NASA Technical Memorandum 4210, pp. 71–73. Washington, D.C.: National Aeronautics and Space Administration.

Thomas, P. C. and Veverka, J.: 1991, *Journal of Geophysical Research* **96** (supplement), 19, 261–268.